Research Performance Progress Report

SUBMITTED TO

U. S. Department of Energy
National Energy Technology Laboratory

WORK PERFORMED UNDER AGREEMENT

DE-FE0013919

Project title: **Mechanisms for Methane Transport and Hydrate Accumulation in Coarse-Grained Reservoirs**

SUBMITTED BY
Prof. Hugh Daigle, PI
Phone: 512-471-3775
Fax: 512-471-9605
daigle@austin.utexas.edu

October 21, 2016

DUNS number: 1702302390000

RECIPIENT ORGANIZATION
University of Texas at Austin
200 E Dean Keeton St., Stop C0300
Austin, TX 78712-1585

PROJECT PERIOD: October 1, 2013 – September 30, 2017

REPORTING PERIOD END DATE: September 30, 2016

REPORT FREQUENCY: Quarterly

Signed:

Hugh Daigle

ACCOMPLISHMENTS

The project **goal** is to show, through numerical modeling, how the transport of methane, and the mechanism by which it is transported, control the development of persistent, massive hydrate accumulations in deep sediments below the seabed. The models will be based on recently collected data from Walker Ridge Block 313 (WR 313) in the northern Gulf of Mexico (Figure 1). To achieve the project goal, the project has been divided into three phases. Phase 1 of the project will focus on modifying an existing reservoir simulator (Sun and Mohanty, 2006) to include microbial methane production, salt mass balance and effects on methane stability, and sedimentation. Additional 1-D modeling will provide constraints on expected rates of methanogenesis. Phase 2 of the project will focus on simulations of dissolved methane migration mechanisms to determine if sufficient flux is available to develop the massive hydrate accumulations observed at WR 313. Phase 3 of the project will focus on simulations of free methane gas migration and recycling of methane in the gas phase as it is buried below the base of the methane hydrate stability zone.

The **objectives** of this project are to define:

1. The dissolved methane flux, organic matter abundance, and time required to develop the accumulations observed at WR 313 by short-distance migration of microbial methane into adjacent coarser-grained layers;
2. The dissolved methane flux and time required to develop the accumulations observed at WR 313 by long-distance, updip migration;
3. Whether there is enough methane in the dissolved phase in the fine-grained sediments to form the observed hydrate deposits or whether a gas phase is present, and if so what the conditions are for three-phase equilibrium;
4. The fate of hydrate that subsides beneath the base of the MHSZ and accumulates as gas, and overpressure generation associated with gas accumulation.

Tasks to be performed
PHASE 1 / BUDGET PERIOD 1
Task 1 - Project management and planning

The Recipient shall work together with the DOE project officer upon award to develop a project management plan (PMP). The PMP shall be submitted within 30 days of the award. The DOE Project Officer shall have 20 calendar days from receipt of the PMP to review and provide comments to the Recipient. Within 15 calendar days after receipt of the DOE's comments, the Recipient shall submit a final PMP to the DOE Project Officer for review and approval.

The Recipient shall review, update, and amend the PMP (as requested by the DOE Project Officer) at key points in the project, notably at each go/no-go decision point and upon schedule

variances of more than 3 months and cost variances of more than 10%, which require amendments to the agreement and constitutes a re-base lining of the project.

The PMP shall define the approach to management of the project and include information relative to project risk, timelines, milestones, funding and cost plans, and decision-point success criteria. The Recipient shall execute the project in accordance with the approved PMP covering the entire project period. The Recipient shall manage and control project activities in accordance with their established processes and procedures to ensure subtasks and tasks are completed within schedule and budget constraints defined by the PMP. This includes tracking and reporting progress and project risks to DOE and other stakeholders.

Task 2 – Reservoir Model Development

The Recipient shall modify an existing general purpose reservoir simulator to include sedimentation, microbial methane production and effect of salt on hydrate equilibrium. The methane equilibrium calculation shall be modified to include changes in water activity due to dissolved salt following the method of Handa (1990). The mass conservation calculation shall be modified to include sedimentation, burial, and changes in porosity over time following the method of Bhatnagar et al. (2007). The initial conditions shall be modified to allow specification of heterogeneous properties (e.g., porosity) throughout the model domain. The boundary conditions shall be modified to allow specification of seafloor sedimentation rate and fluid flux. The Recipient shall verify code modifications with benchmark comparisons of performance with published simulation results (e.g., Bhatnagar et al., 2007).

Task 3 – 1-D Modeling of Microbial Methanogenesis

Concurrently with Task 2, the Recipient shall start with a 1-D reaction-transport model that will follow the burial by sedimentation of a sand layer surrounded by fine-grained sediments. The time-dependent modeling shall track the evolution of gas hydrate formation in the sand layer and shall provide more accurate estimates of the time scales and of the gas hydrate quantities associated with short migration. The methane hydrate stability conditions shall include the effect of pore size in the sand and fine-grained layers following the method of Malinverno (2010). The rate and spatial distribution of microbial methanogenesis shall be constrained by data from scientific ocean drilling expeditions (DSDP, ODP, IODP). The results of this task shall provide first-order constraints on rates of methanogenesis which shall be used as inputs to subsequent tasks (4.1, 4.3, 5.1, 5.2).

PHASE 2 / BUDGET PERIOD 2
Task 4.1 – Short Migration of Dissolved Methane

The Recipient shall investigate short migration of dissolved methane, in which methane generated in fine-grained sediments within the MHSZ is transported by diffusion into adjacent coarse-grained layers in which it forms concentrated hydrate deposits. The simulator developed in Task 2 shall be used for this task. The model domain shall consist of dipping sand layers surrounded by fine-grained sediments. This domain shall be designed to approximate the geometries observed at WR313 with sediment physical properties defined from logs or analog data. Rates of microbial methanogenesis and fluid flow shall be altered to determine the effect each has on the resulting hydrate distribution and time required for accumulation. The model results shall be used to determine the time scale of short migration at WR313, and the distribution of hydrate resulting from short migration.

Task 4.2 – Long Migration of Dissolved Methane

The Recipient shall investigate long migration of dissolved methane, in which dissolved methane is transported by advection from a distant source to the MHSZ. The investigation shall use the simulator developed in Task 2. The model domain shall consist of dipping sand layers surrounded by fine-grained sediments, and shall be designed to approximate the geometries observed at WR313. The model shall assume no local methane generation in the MHSZ and pore water entering the MHSZ with a methane concentration equal to the local solubility. Fluid flux shall be determined assuming that fluid flow is driven by overpressures to due high sedimentation rates (Gordon and Flemings, 1998). The Recipient shall explore the time scale associated with long migration by determining how long is required for fluid flow to form hydrate deposits comparable to those observed at WR313. The Recipient shall additionally simulate situations in which active fluid flow ceases after some time, and investigate how the hydrate that is formed evolves after cessation of fluid flow.

Task 4.3 – Assessment of Flux Associated with Dissolved Methane Migration

The Recipient shall use the model results from Tasks 4.1 and 4.2 to assess the methane flux associated with methane migration in the dissolved phase by either long or short migration. The different scenarios modeled in Tasks 4.1 and 4.2 shall be analyzed to determine methane flux from each migration mechanism, and the time scales and hydrate volumes produced by each. The analysis results shall be compared to the observed hydrate accumulations at WR313 and the age of the host sediments to determine whether migration of dissolved methane could have produced the observed hydrate accumulations.

PHASE 3 / BUDGET PERIOD 3
Task 5.1 – Assessment of Methane Budget Required for Presence of Gas Phase

The Recipient shall use the results of Tasks 4.1 and 4.2 to define methane availability from local, microbial sources as well as deeper sources (thermogenic or microbial). The phase equilibrium implemented in the 3-D model in Task 2 shall be used to determine local solubility within the model domain and determine the amount of methane that may be present as a gas phase. The results of this task will be used to place limits on gas availability in Tasks 5.2 and 5.3.

Task 5.2 – Free Gas Migration

The Recipient shall apply a previously established model of hydrate formation (multiphase-flow-controlled, nonequilibrium, neglecting transport of salinity and latent heat) to assess whether the gas phase accumulated beneath the MHSZ can contribute significantly to hydrate saturations within the MHSZ. The Recipient shall evaluate the conditions under which the accumulated gas phase drains into coarse-grained sediment. Having identified those conditions, the Recipient shall evaluate the geologic setting (dip angle, petrophysical properties and multiphase flow properties of the sediment) for which significant updip migration of the gas phase can be expected. The Recipient shall apply the hydrate formation model to geologic settings with significant expected migration to determine the hydrate saturation distribution in the updip direction. The model shall be tested for ranges of the two competing rates (namely, rate of gas accumulation at base of MHSZ and rate of hydrate formation from gas phase and water phase in the MHSZ). The Recipient shall additionally determine the pressure, temperature, and salinity conditions that will permit short migration of a gas phase within the MHSZ. The predicted saturation distributions shall be compared to observations (magnitude of hydrate saturation and its lateral extent) within coarse-grained layers at WR313. If hydrate is predicted to form in the same location and same volume as the accumulations observed at WR313, the Recipient shall determine whether the conditions that give agreement are geologically plausible, and the Recipient shall compare the flux of methane in the gas phase to the fluxes of methane by other mechanisms to be determined in Tasks 4.1 and 4.2. If the rates of methane delivery and time scale of hydrate accumulation are consistent with the accumulations observed at WR313, the Recipient shall use the results to guide the inclusion of free-gas migration phenomena into the full-physics 3D simulations of Task 5.3.

Task 5.3 – Methane Recycling at the Base of the MHSZ

The Recipient shall use the reservoir model developed in Task 2 to evaluate the fate of hydrate that moves below the base of the MHSZ as a result of sedimentation. In particular, the Recipient shall examine subsidence of dipping, hydrate-bearing sands of the type encountered at WR313. The Recipient shall model burial of a dipping sand layer through the base of the MHSZ in 3 dimensions. The Recipient shall test different scenarios of sedimentation rate, hydrate saturation in sand layers, and deep methane flux to evaluate gas accumulation below the MHSZ, supply of methane to the base of the MHSZ, and overpressure generated by the accumulation of a

connected gas column. The gas column will be considered connected when it overcomes a percolation threshold of roughly 10% of the pore volume (England et al., 1987). Gas phase pressure shall be computed from gas column height and estimates of capillary pressure from analog sediments (e.g., Blake Ridge; Clennell et al., 1999). The potential to fracture overlying sediments shall be investigated by comparing the resulting pore pressure to the total vertical stress and the minimum horizontal stress.

Milestone Status Report

1.A Title: PMP submission
Planned Date: 4 December 2013
Completed Date: 22 November 2013
Verification Method: Submission of final Project Management Plan to DOE within 65 days of start of project.

1.B Title: Project kick-off meeting
Planned Date: 29 December 2013
Completed Date: 7 November 2013
Verification Method: Meeting held within 90 days of start of project.

1.C Title: Sedimentation, microbial methane production, salinity effect implementation
Planned Date: 30 June 2014
Completed Date: 30 June 2014
Verification Method: Implementation of sedimentation, microbial methane production, salinity effect on hydrate stability in 3-D model.

1.D Title: Benchmarking of numerical model against published results
Planned Date: 31 March 2015
Completed Date: 31 March 2015
Verification Method: Simulation results match those obtained from other simulators in 1-D and 2-D (e.g., Bhatnagar et al., 2007; Chatterjee et al., 2011) within 1% in time and hydrate saturation using the same input parameters.

1.E Title: Development of time and methanogenesis constraints for future modeling
Planned Date: 31 March 2015
Completed Date: 31 March 2015
Verification Method: Development of a model that includes time-dependent changes in methane stability in a dipping, subsiding sand layer but matches the results of Cook and Malinverno (2013) for steady-state conditions.

2.A Title: Completion of short migration modeling
Planned Date: 30 September 2016
Completed Date: 30 September 2016
Verification Method: Completion of simulations to evaluate conditions necessary for development of massive hydrate deposits by short migration.

2.B Title: Completion of long migration modeling
Planned Date: 30 September 2016
Completed Date: 30 September 2016
Verification Method: Completion of simulations to evaluate conditions necessary for development of massive hydrate accumulations by long migration.

2.C Title: Quantification of methane flux in the dissolved phase
Planned Date: 30 September 2016
Completed Date: 30 September 2016
Verification Method: Quantification of methane flux associated with methane migration in the dissolved phase by either long or short migration and comparison with existing estimates of methane flux in the northern Gulf of Mexico such as those presented in Frye (2008).

3.A Title: Quantification of methane availability and expected quantities of gas
Planned Date: 30 September 2017
Verification Method: Quantification of amount of methane required to form a free gas phase and comparison with existing estimates of methane flux in the northern Gulf of Mexico such as those presented in Frye (2008).

3.B Title: Completion of free gas migration models
Planned Date: 30 September 2017
Verification Method: Determinations of methane flux and time necessary to reproduce observed hydrate accumulations at WR313 by migration of free gas.

3.C Title: Completion of modeling efforts to assess methane recycling
Planned Date: 30 September 2017
Verification Method: Completion of simulations to assess rates of gas accumulation beneath MSHZ and effect on gas migration and overpressure generation.

What was accomplished under these goals?

Major activities

We performed sophisticated 1D, 2D, and 3D modeling to investigate hydrate formation at WR313.

Model setup

One- and two-dimensional simulations were performed on a small scale to assess the impact of methane diffusion on gas hydrate distributions within and immediately surrounding a thin sand layer as it is buried through the GHSZ. In these simulations, we adopt a Lagrangian reference frame: boundary conditions change through time in the simulation to reflect increasing pressure and temperature within a small domain describing the burial of an individual sand layer. The 1D simulation control volume is depicted in Figure 1.

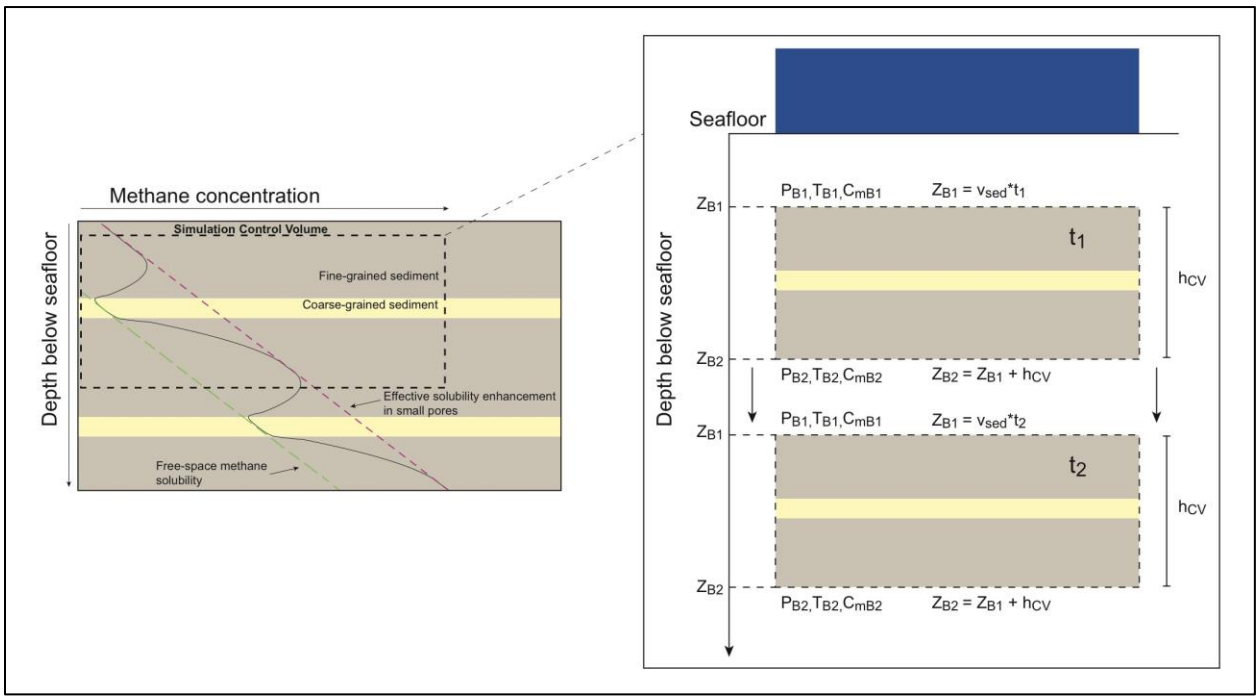

Figure 1. A fully developed methane concentration profile in a repeating sequence of alternating fine- and coarse-grained sediments with the free space methane solubility (dashed green line) and clay layer methane solubility (dashed magenta line) superimposed. The control volume in 1D centers around a sand layer and is buried deeper beneath the seafloor with time. Boundary conditions change correspondingly.

Temperature boundary conditions (TB1 and TB2 in Figure 1) are set according to the seafloor temperature and the geothermal gradient, pressure boundaries (PB1 and PB2) are hydrostatic,

depths (ZB1 and ZB2) are determined by the sedimentation rate (vsed) and the simulation time (t1 and t2). Boundary values for methane concentrations (CmB1 and CmB2) before hydrate is present in the system are set equal to the methane concentrations in the adjacent interior cell at the previous time step plus the methane input at the depth of the boundary due to methanogenesis. When hydrate is present, methane concentrations on the boundaries are set equal to the methane concentrations in the adjacent interior cell at the previous time step.

In 2D, the domain is discretized into an array of right rhombic prisms; the gravity vector is rotated to simulate a dipping sand (Figure 2a). In 3D, a static system buries sand at time steps that depend on grid discretization (Figure 2b). One- and two-dimensional simulations are limited in that they cannot describe regional-scale gas hydrate distribution patterns; 1D simulations illustrate hydrate distributions within a sand layer itself, while 2D simulations yield insight into average hydrate saturation variations along a short length of a single thin sand. However, these simulations provide results at a resolution not possible in 3D simulations due to computational limitations.

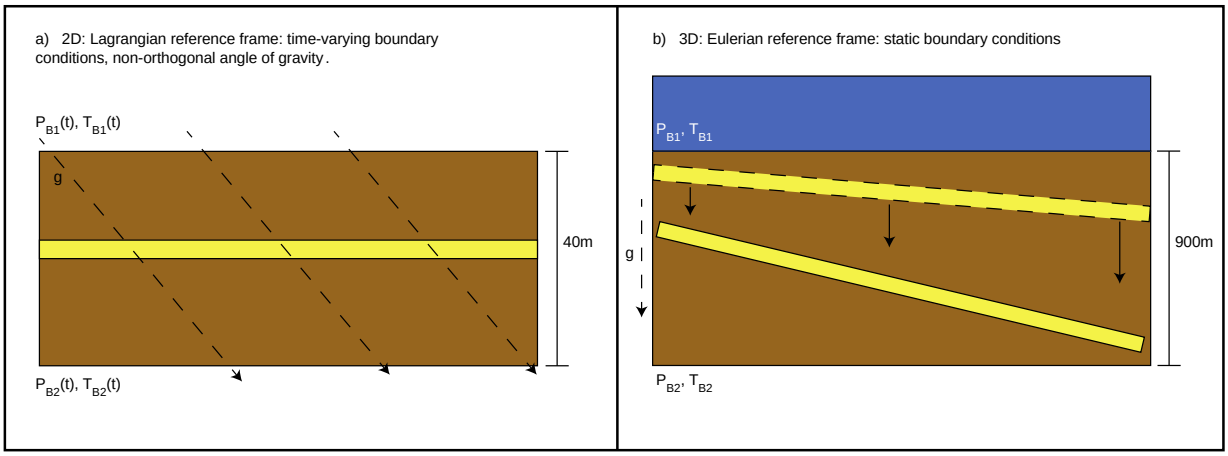

Figure 2. a) A moving (Lagrangian) reference frame is used for 1D and 2D simulations of hydrate distributions within and around single sand layers, while b) a static (Eulerian) reference frame is implemented in this study for 3D basin-scale simulations.

In 1D simulations performed in this study, all grid blocks are 0.6m thick. The thickness of the entire sand layer varies from 1.8 m to 18 m with 25.5 m of clay both above and below the sand layer, for a total domain length of between 52.8 m and 69 m. In 2D, the sand thickness is discretized as one 3.6 m grid block. The downdip length of the sand layer in these simulations is set at 100 m, discretized into 20 grid blocks. Three-dimensional simulations are performed in an Eulerian reference frame (Figure 2b): hydrostatic pressure conditions and a constant geothermal gradient are imposed on 11250 grid blocks (50 in the downward z-direction and 15 in each lateral dimension) discretizing a basin system that spans 118.74 cubic kilometers. This resolution

yields a sand grid block thickness of 18.3 m, which is about 5 times the thickness of the individual sand unit modeled in 2D. Therefore, because of computational limitations on grid discretization, 3D simulations are not able to resolve hydrate-free zones immediately surrounding sand layers; nor can they depict gas hydrate distributions within individual sands. They do, however, illustrate regional gas hydrate distribution trends across multiple dipping, non-planar sands.

Incorporating heterogeneity from well logs, laboratory measurements, and seismic data
The simulation environment was developed to incorporate interpreted seismic horizons directly as input information to build the structure of the simulated reservoir. It then uses this data when building the structure of the grid to calculate spatial variations in sediment permeability, porosity, and pore size. Three-dimensional simulations presented here use interpreted seismic data to define sand geometries; all simulations adopt an empirical porosity-depth trend due to compaction formulated for Walker Ridge sediments from log data as follows:

$$\phi(z) = 0.35e^{-0.016z} + 0.37e^{-0.00019z}, \qquad (1)$$

where ϕ is the sediment porosity and z is the depth beneath the seafloor in meters. This compaction trend is applied to both the sand and the clay lithology. Future work could improve upon these simulations by applying different compaction trends to different lithologies, but the porosity data presented by Daigle et al. (2015) indicate that the difference between sand and clay porosities is significant only in the first 100 meters below seafloor (mbsf) at Walker Ridge.

In simulating diffusive methane transport within a thin coarse-grained sand on a small scale, pore size distributions have a strong impact on gas hydrate growth potential. This is because the magnitude of the solubility change of methane in water due to changes in pressure and temperature across an individual sand layer is comparable to (and even outweighed by) the solubility change between the largest and smallest sediment pores. In a porous medium containing a distribution of pore sizes, the nonwetting gas hydrate phase will preferentially fill large pores first before filling smaller pores, a phenomenon resulting from the solubility increase due to the Gibbs-Thomson effect (Liu and Flemings, 2011). Therefore, as the sediment pore space fills with hydrate, progressively larger amounts of aqueous methane are required to precipitate hydrate in the pore space.

Incorporating this phenomenon is also important from the perspective of minimizing resolution-dependent hydrate growth across lithologic discontinuities. For a discrete system containing sand and clay intervals defined by a single pore size, if the grid discretization is refined to resolve smaller volumes at the clay-sand boundary, the same methane mass flux from surrounding clay to the edge of a sand grid block will produce higher saturations of gas hydrate at the sand's edges than in a lower resolution model. This can lead to practical simulation difficulties in 1D (when

ignoring fracturing potential) and inconsistencies between grids of varying resolution, whereby hydrate saturations can reach (or surpass) 100% of the pore space available in the sand layer, and the permeability at a sand's edge can drop to 0.

In high resolution simulations, pore water methane solubility can instead be reformulated not only as a function of pressure, temperature, salinity, and single pore characteristics but additionally as a function of the pore size distribution within a grid block. While sands are generally considered to contain large pores with negligible influence of pore curvature effects on aqueous methane solubility, we show that a broad pore size distribution within a sand layer that is centered at a relatively small median pore size can actually significantly redistribute hydrate toward the center of the sand in comparison to a sand layer described by a single pore size or a narrow pore size distribution (Figure 3).

To incorporate this effect we describe an effective pore radius that governs equilibrium hydrate precipitation, which decreases with increasing gas hydrate saturation. A decreasing effective pore radius leads to an enhancement in the Gibbs-Thomson effect within hydrate-bearing pore space. Using well log and MICP data on samples recovered from JIP Leg 1 Keathley Canyon 151 in the Gulf of Mexico, we approximate that the sand layers can be described by a lognormal pore size distribution with a median pore radius r_m and standard deviation σ_r (Bihani et al., 2016); we then formulate a synthetic function expressing effective pore radius influencing three-phase equilibrium in the sand layer as a function of pore-filling gas hydrate saturation. First, we define a lognormal cumulative distribution function in terms of incremental (effective) pore radius, r_e, total pore volume, V_{tot}, and cumulative volume in pores smaller than r_e, V:

$$\frac{V}{V_{tot}} = 0.5\left(1 + erf\left[\frac{\ln r_e - \mu}{\sqrt{2}\sigma}\right]\right), \quad (2)$$

$$\mu = \ln\left(\frac{r_m}{\sqrt{1+\frac{\sigma_r^2}{r_m^2}}}\right), \quad (3)$$

$$\text{and } \sigma = \sqrt{\ln\left(1+\frac{\sigma_r^2}{r_m^2}\right)}, \quad (4)$$

where μ is the location parameter and σ is the scale parameter of the distribution.

Because this represents the volume fraction of free pore space (increasing hydrate saturations are associated with decreasing effective pore radius), Equation 2 can be rewritten in terms of pore filling hydrate saturation as follows:

$$1 - S_h = 0.5\left(1 + erf\left[\frac{\ln r_e - \mu}{\sqrt{2}\sigma}\right]\right), \quad (5)$$

where S_h is the fraction of pore space occupied by gas hydrate. Solving for effective pore radius as a function of hydrate saturation, the equation is rearranged as follows and incorporated into simulations:

$$r_e = \exp\left(\sqrt{2}\sigma erf^{-1}(1 - 2S_h) + \mu\right), \quad (6)$$

where r_e is the effective pore radius governing methane solubility of the next pore in which hydrate can precipitate. This effective pore radius is then used in the Gibbs-Thomson equation to describe the evolution of the three-phase equilibrium pressure with changing hydrate saturation in the sand layer. We apply this process only to sands in the simulation; we ignore pore size distribution effects in the clay layers because gas hydrate is not typically observed in a pore-filling habit in clay sediments in the Terrebonne basin. Rather, hydrate tends to fill clays in fracture or vein networks, and over a regional scale, gas hydrate saturations as a percentage of clay pore space tend to be small (<5%).

Results

In all simulations reported in this study, a binary system of sand and clay lithologies is considered: sands are characterized in 1D and 2D simulations by pore size distributions and in 3D by a single pore radius, rsand, defining aqueous methane solubility. In all simulations, the clays are described by a single pore radius (rc,max in 1D and 2D, and rclay in 3D), and microbial methanogenesis is only active in the clay lithology.

We simulate a Walker Ridge-like system, in which a thick, ~2 km water column and a low geothermal gradient contribute to a thick GHSZ. In 1D and 2D, the reaction rate of methanogenesis, λ, and the organic carbon content at the SMT, α_{SMT}, are approximated following Malinverno (2010); the depth of the SMT, z_{SMT}, is estimated based off of data at Keathley Canyon (Kastner et al., 2008) and Alaminos Canyon (Smith et al., 2014). The sand layers are buried to a maximum depth of 900 mbsf and are therefore completely contained within the GHSZ throughout the duration of the simulations. Physical properties used in all simulations are shown in Table 1.

One-dimensional Lagrangian simulations

One-dimensional simulations were performed in this study to resolve the hydrate distribution patterns within thin sands buried through the GHSZ. The distribution of gas hydrate within and immediately surrounding the thin sand is tracked in a moving reference frame with time-varying boundary conditions. At the bottom of the domain, a compaction-driven flux boundary condition diminishes with burial as the change in porosity of the system with burial approaches zero. The top of the domain is kept at a constant pressure corresponding to hydrostatic pressure at the depth of the boundary. While this pressure may not be exactly hydrostatic (if fluid is moving upward above the domain), the magnitude of any overpressure in this system due to compaction flux has a negligible impact on methane solubility throughout the system. Boundary temperatures are fixed along a geothermal gradient, and methane concentration across the top and bottom boundaries is held constant. The simulation boundaries are placed sufficiently far from the sand such that hydrate growth in the sand is separated from hydrate in clays by hydrate-free zones.

Pore Size Distribution Effects on Gas Hydrate Growth in Sands

Within a single horizontal sand layer of finite thickness, aqueous methane solubility increases from the top of the sand to the bottom, as the temperature in the sand is higher at its base. In thin sands, the gradient in solubility is smaller than in thick sands because the temperature difference is smaller, and the solubility-depth trend is nonlinear and locally convex. When a gradient in aqueous methane solubility between a sand and surrounding clays drives diffusive methane transport toward the sand layer, gas hydrate accumulates in high saturations at the edges of the sand. If the concentration gradient within a sand layer is insignificant in comparison to the sand-clay methane solubility gradient, hydrate will only accumulate in significant saturations at the edges of the sand with minimal diffusive transport toward the sand's center.

One way to enhance the solubility gradient within a sand layer as a function of hydrate saturation is to incorporate pore size distribution effects relevant to pore-filling hydrate accumulations (Figure 3). Since hydrate growth in clays tends to fracture-fill, we interpret simulated hydrate saturations in the bounding clays as fracture filling and therefore do not apply pore size distribution effects to the clay lithology. If solubility is lowest in the largest pores, and if no pores can fill with interstitial hydrate, then fracture-filled hydrate growth should be governed by the methane solubility of the largest clay pore. Thus, we define a maximum pore size governing hydrate growth in the clay intervals, r_{cmax}.

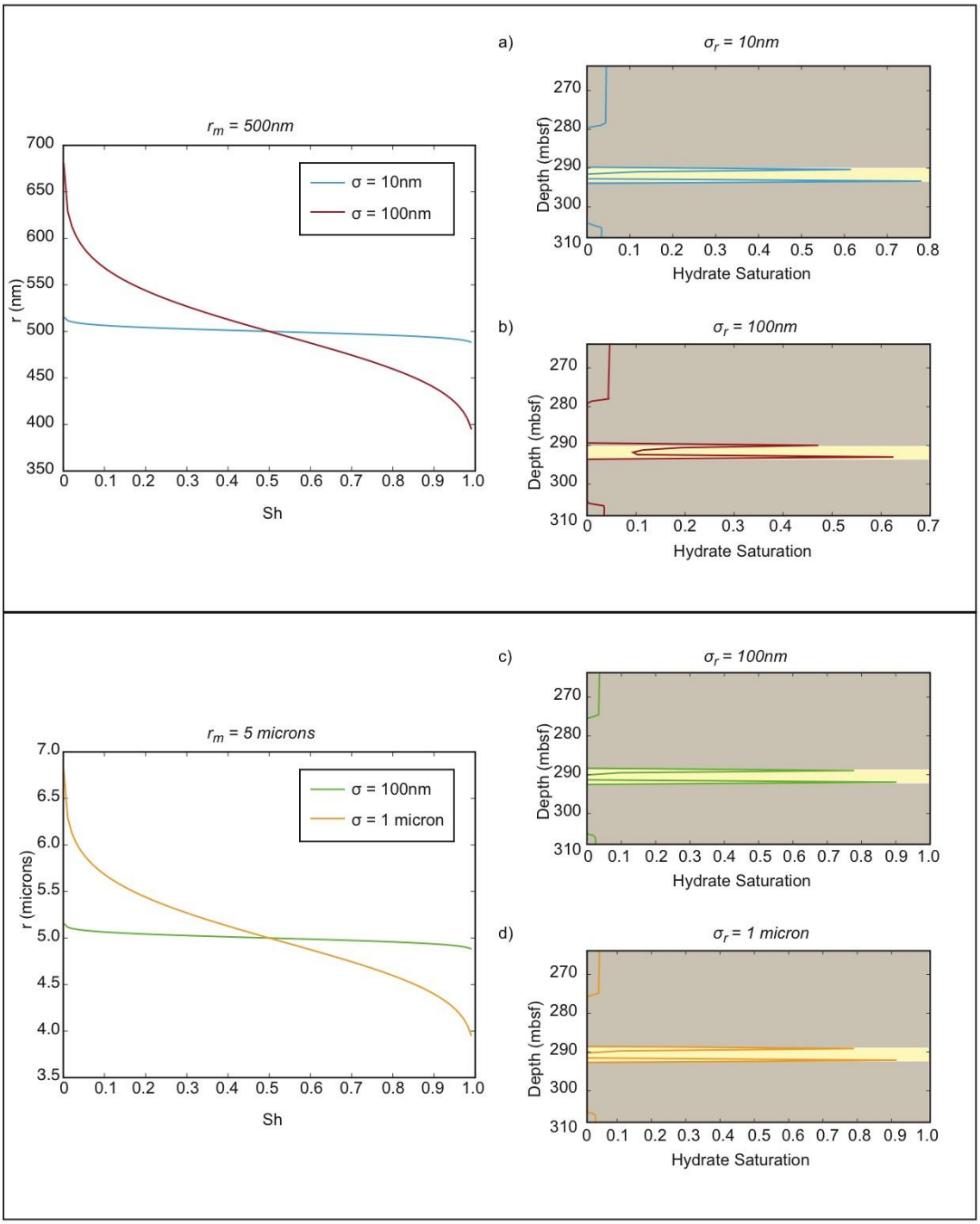

Figure 3. The gas hydrate distribution impact within a thin sand under four pore size distribution scenarios: a) low median pore size and low standard deviation in pore size; b) low median pore size and high pore size standard deviation; c) high median pore size and low standard deviation; d) high median pore size and high standard deviation.

As is depicted in Figure 3, the distribution of gas hydrate within a thin sand depends heavily on the sand's pore size distribution. If the sand exhibits a low standard deviation in pore size (Figure 3a, 3c), gas hydrate is unable to accumulate in massive quantities at the center of the sand because the aqueous methane solubility gradient within the sand is minimal; hydrate growth in a sand characterized by larger pores (Figure 3d) fills with greater amounts of hydrate (nearly 100% of the pore space) at the sand's edges. Contrastingly, in a sand layer characterized by a broad pore size distribution and a relatively low median pore size closer to that of a silty lithology (Figure 3b), hydrate growth toward the center of the sand can reach upward of 20% of the average saturation at the layer's edges. This is not possible, however, in a sand containing entirely large pores (Figure 3d).

These results suggest that although a strong sand-clay solubility contrast is required to drive significant diffusive flux of methane from clays to sands, gas hydrate cannot evenly distribute throughout the sand layer unless there exists a significant gradient in aqueous methane solubility within the sand layer itself. Within a thin layer at high resolution, resolving lithologic heterogeneities within the layer should therefore have a significant impact on methane hydrate distributions within the layer.

Gas Hydrate Distribution Patterns in a Sand Buried through the GHSZ

We track the evolution of a gas hydrate bearing sand layer in a Walker Ridge-like gas hydrate system by defining r_{cmax} following Bihani et al., 2015 in the bounding clay material. Because the rate of change in hydrate saturation within a sand grid block depends on the dissolved methane concentration gradient and inversely on grid discretization (Rempel, 2011), we impose a lognormal pore size distribution whose median pore size is determined experimentally (Bihani et al., 2015) but whose pore size at 99.7% hydrate saturation is equivalent to rc,max. This ensures that as hydrate saturation increases in the sand layer, the gradient in methane concentration between the sand and surrounding clay tends toward zero, imposing a limit on the rate at which hydrate saturations can increase via diffusive methane transport. Figure 4 depicts a schematic of a 1D simulation in which one thin sand layer (3.6 m thick) is buried through a microbially active GHSZ at a constant sedimentation velocity (vsed).

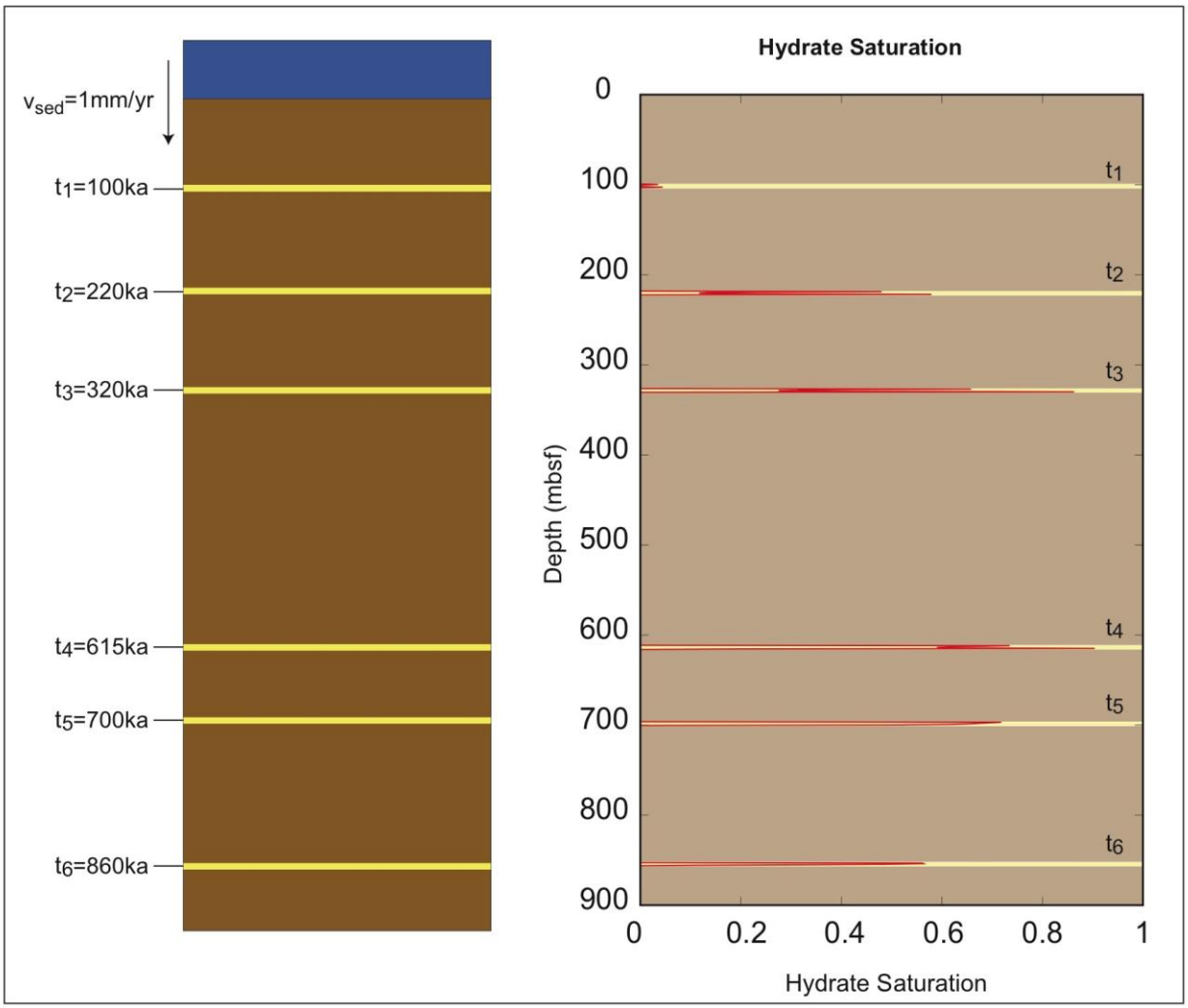

Figure 4. One-dimensional time-series evolution of hydrate saturation profiles within a single thin sand layer (3.6 m thick) in a Lagrangian reference frame as it is buried through the hydrate stability zone, incorporating capillary effects on diffusive aqueous methane concentration gradients.

As shown in Figure 4, in a microbially active gas hydrate system with only compaction-driven upward fluid flow, a thin sand layer tends to diffusively soak up methane from surrounding clay material as it is buried. The sand-clay solubility contrast promotes diffusive methane transport to the sand layer; the presence of this gradient requires that hydrate-free zones separate a hydrate-bearing sand from hydrate-bearing clay above and below it. Hydrate saturations in the sand layer tend to increase over time while the supply of methane via microbial methanogenesis in the clays outpaces hydrate dissolution due to increasing solubility with burial. Once the input of methane from microbial activity diminishes such that there is net hydrate dissolution in the bounding

clays, hydrate growth is still possible in sands until all the hydrate in the surrounding clay material has dissociated.

Figure 5 highlights three observable trends in the gas hydrate growth pattern within a sand layer (6 m thick) as it is buried through the GHSZ. At early time (Figure 5a), hydrate is present in clays above and below the sand layer. The gradient in aqueous methane concentration is fixed by the solubility of methane in pore water above and below the hydrate-free zones, and diffusive methane transport is directed entirely toward the sand layer. Hydrate accumulates at a faster rate at the base of the sand than at the top. This is due to a steeper sand-clay solubility gradient at the bottom of the sand (as evidenced by the aqueous methane concentration gradients through the hydrate-free zones) as well as upward advective compaction flux. As hydrate saturations increase at the edges of the sand, the effective sand pore radius decreases and a diffusive gradient within the sand allows for methane transport toward the sand's center.

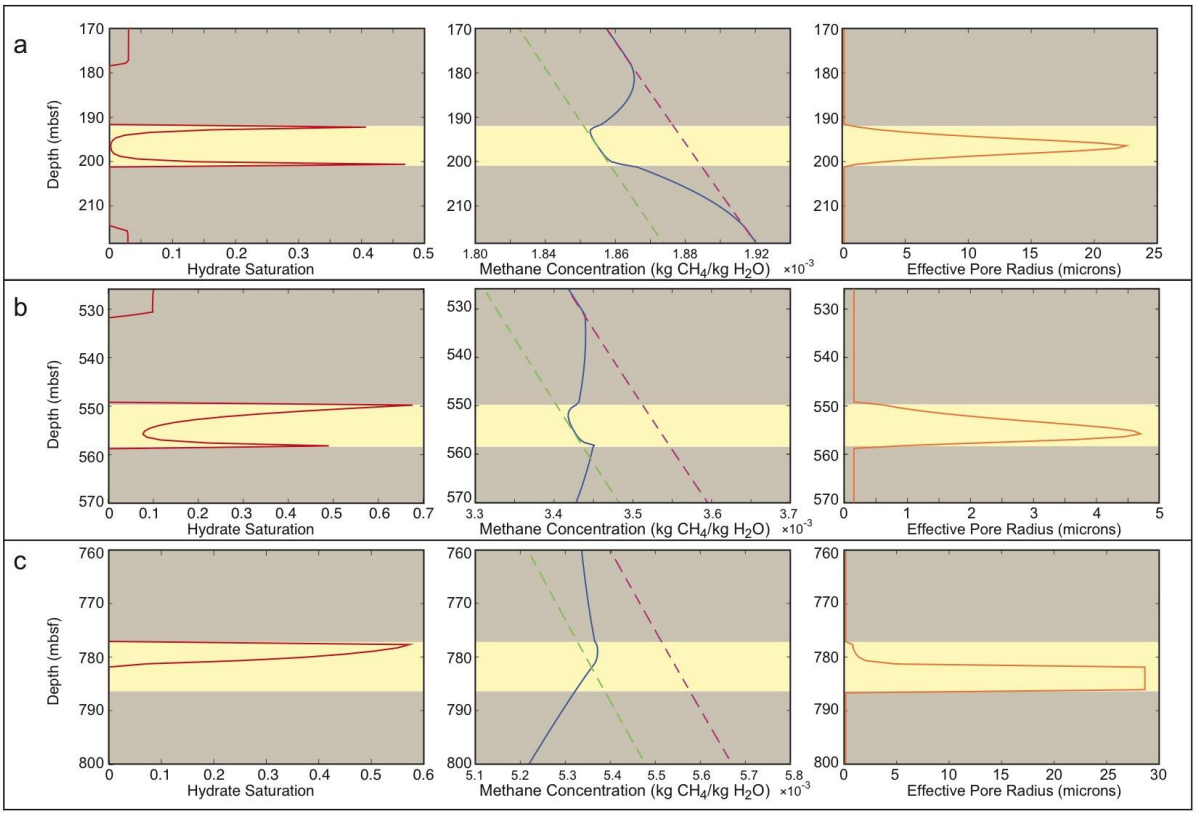

Figure 5. Patterns of gas hydrate distribution (red), dissolved methane concentration (blue), and effective pore radius (orange) governing methane solubility within a 6 m-thick sand layer as it is buried through the GHSZ. A dashed green line indicates bulk aqueous methane solubility, and a dashed magenta line indicates the effective aqueous methane solubility in clay pores. The sand layer is highlighted in yellow, and the bounding clay is highlighted in brown.

Once the influx of microbial methane is insufficient to cause further hydrate growth in the clay layer, hydrate contained within the clay beneath the sand layer first begins to dissociate. Because hydrate is still present in the clay, however, an aqueous methane concentration gradient between the bounding clay and the sand layer still exists, so gas hydrate dissolving in the clay layer feeds hydrate that is present in the sand, preserving hydrate in the sand from dissociation with burial. Once all of the hydrate in the clay beneath the sand layer has dissociated (Figure 5b), hydrate begins to dissociate from the bottom of the sand layer. Although a methane concentration gradient drives diffusive flux out of the base of the sand, a concentration gradient also drives diffusive methane transport from the base of the sand to its center. Net methane migration from above is still directed toward the center of the sand. Hydrate growth can therefore still occur at the top of the sand layer if hydrate still exists in the bounding clay above the sand (or as long as the methane concentration in this region exceeds the solubility of methane in the pore water of the sand). Once the hydrate within the clay above the sand and at the base of the sand fully dissociates (Figure 5c), hydrate on the upper sand boundary proceeds to dissolve. In this case, the methane concentration gradient drives diffusive methane transport out of the sand from above and below.

Intriguingly, these simulations illustrate the potential for gas hydrate dissociating within clay over time to feed and preserve the hydrate existing within sand layers against dissociation while burial increases aqueous methane solubility. This suggests that if hydrate deposits are observed to occur in any quantity within clays at depth in close proximity to thin sands, hydrate grown in the sands could have been preserved with burial as the sands soaked up dissolved methane from dissociating hydrate in clays. In the fracture-hosted clay hydrate deposits typically observed in the Gulf of Mexico, this means that deep hydrate fractures in clays could be preserving large accumulations of hydrate in nearby sands.

The Effect of Layer Thickness on Gas Hydrate Distributions within a Sand

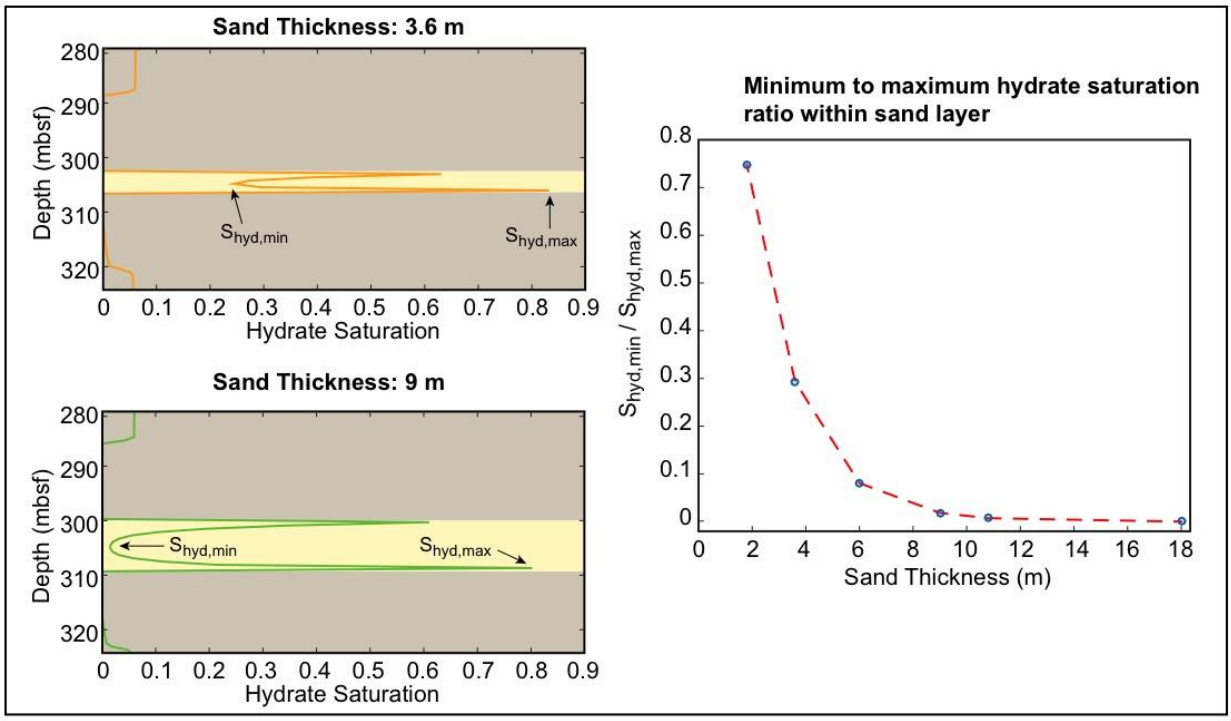

Figure 6. A comparison of minimum to maximum hydrate saturation within a sand for varying thicknesses of sand layers bounded by clays. The sand layer is highlighted in yellow, and the clays are highlighted in brown.

For a given pore size distribution within a sand layer and a constant total methane mass flux from the bounding clay intervals to the sand layer, the distribution of gas hydrate within a coarse-grained sand layer depends on the sand layer thickness. Figure 6 compares the accumulation of gas hydrate within a sand layer at a particular depth for different sand thicknesses, holding constant the grid discretization and the amount of methane generated through microbial methanogenesis in the bounding clays.

For small sand thicknesses (the 3.6 m sand in Figure 6), the aqueous methane concentration difference between a sand's edge and its center is enhanced due to significant hydrate growth decreasing the effective pore radius at the sand's edge, which drives diffusive methane flux toward the sand's center. The relatively short distance (in comparison to a thicker sand, as in the 9 m sand of Figure 6) from the sand's edges to its center creates a strong concentration gradient that generates significant hydrate accumulations in the center of the sand. Contrastingly, as the distance from the edge of a sand to its center increases, the methane concentration gradient from the edge to the center decreases, which in turn decreases the amount of methane that can be transported from the edge of a sand to its center. The ratio of the minimum to maximum hydrate saturation within a sand (Figure 6) therefore decreases with increasing thickness and eventually reaches 0 at a finite sand thickness.

Simulation Comparisons to Observations at WR313

In the Terrebonne Basin, the JIP Leg 2 drilled two wells, Hole WR313-G and Hole WR313-H, targeting two reservoir sand units near the base of the gas hydrate stability zone, the Blue sand and the Orange sand (Boswell et al., 2012; Frye et al., 2012).

In Hole WR313-G, logging-while-drilling (LWD) measurements revealed that the Blue sand unit contains sandy layers interbedded with clays. Sediment with higher concentration of clay tends to contain larger amounts of radioactive elements, and thus, have higher API values on the gamma ray log (Figure 7a). Sand sediments generally contain less radioactive elements and exhibit lower API values. The Blue sand unit occurs from 825-873 msbf, with ~25 m of hydrate bearing sand (Figure 7). Gas hydrate saturations within the sand layers in the Blue sand unit are highly variable, and appear to range from as low as 10% in some thin sand laminations, to over 80% in the thicker laminations; gas hydrate saturation calculations follow the technique as outlined in Cook and Waite (2016).

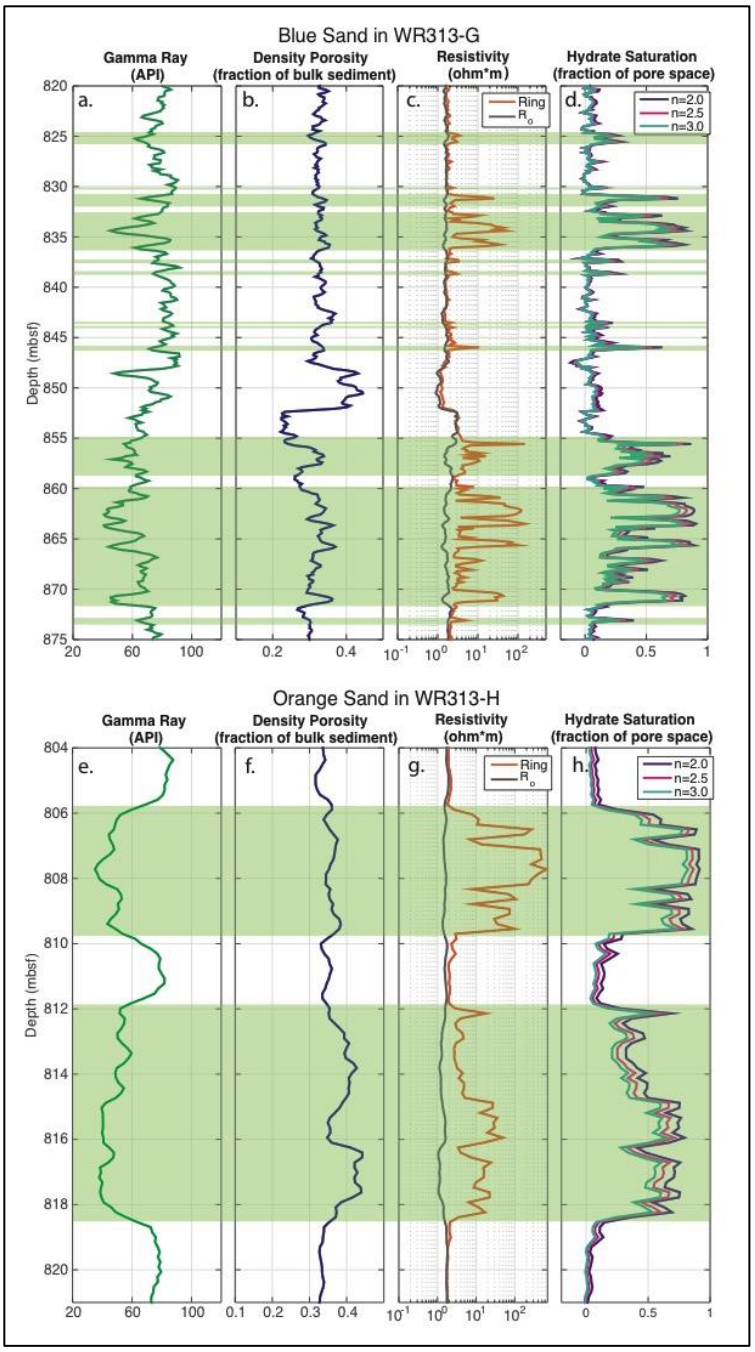

Figure 7. Measured and calculated logs from Hole WR313-G Blue sand unit (a-d) and Hole WR313-H Orange sand unit (e-h) in meters below seafloor (mbsf). Interpreted hydrate-bearing sands are highlighted in green. Tracks a and e show the measured gamma ray log, which indicates sandier layers to the left (lower API) and clay rich layers to the right (higher API). Tracks b and f show the density porosity, which is corrected for the hydrate saturation. The measured Ring resistivity is shown in tracks c and g and the calculated hydrate saturation is presented in tracks d and h. Calculated hydrate saturation and density porosity follow the process outlined in Cook and Waite (2016, in review).

Our total hydrate bearing thickness for the Blue sand is significantly larger than interpreted by Boswell et al., (2012) and Frye et al., (2012), whom reported a total thickness of only 9 m and 11 m of hydrate bearing sand, respectively. We disagree with the conservative estimates of Boswell et al., (2012) and Frye et al., (2012), who did not count intervals with resistivity 1 to 3 ohm-m above background resistivity (Ro) as hydrate-bearing. These low resistivity increase correspond to low to moderate gas hydrate saturation hydrate (~10-40%). These low resistivity layers are most likely hydrate, however, as these intervals have no associated increase in density (Figure 7) and most correspond to an increase in compressional velocity.

The Orange sand in Hole WR313-H is contained exclusively in two lobes, a 4 m lobe starting just above 806 mbsf and a 6.5 m lobe beginning at 812 mbsf, for a total of 10.5 m of gas hydrate bearing sand (Figure 7). In this sand, the lowest calculated gas hydrate saturation is 20%, and the highest is nearly 90%. Again, our interpreted Orange sand is thicker than the value reported by Frye et al., (2012) though only by 2.5 meters. Our Orange sand thickness of 10.5 m aligns with the thickness interpreted by Cook et al., (2012). Resistivity modeling by Cook et al., (2012), demonstrates that the thin clay interbeds in Hole WR313-H interpreted by Boswell et al (2012) as water saturated are likely not water saturated clays, but are more likely to be thin, lower saturation, hydrate-bearing beds.

A number of thin sand layers ($\geq$ 3m) were also identified throughout Holes WR313-G and WR313-H, some sand layers contain gas hydrate and other sand layers are water-saturated. One 2.5 m sand that generated a lot of interest, called Unit A by Boswell et al. (2012) and Cook and Malinverno (2013), appears near 290 mbsf within a 150 m thick clay rich unit containing gas hydrate filled fractures. To continue with the tradition of sands being named a color in the Terrebonne Basin, we have renamed this 2.5 m sand the Red sand. The Red sand has a combination of interesting characteristics, for example, the hydrate in the sand is concentrated near the top and bottom of the sand, leaving the center water-saturated. Surrounding the sand, a hydrate-free zone persists within the bounding clays for several meters before hydrate is again observed in fractures. These features lead Cook and Malinverno (2013) to propose that the Red sand could be filled with hydrate as the result of diffusive methane migration from the surrounding clay, termed short migration.

We compare this observational data to 1D numerical modeling by plotting the average hydrate saturation contained within a modeled sand interval as a function of sand thickness for varying depths of burial (Figure 8). Simulations indicate that for given environmental conditions (water depth, geothermal gradient, pore size distributions, microbial methanogenesis parameters, etc), the average hydrates saturation within a coarse-grained sand layer buried through the GHSZ is inversely proportional to the sand's thickness.

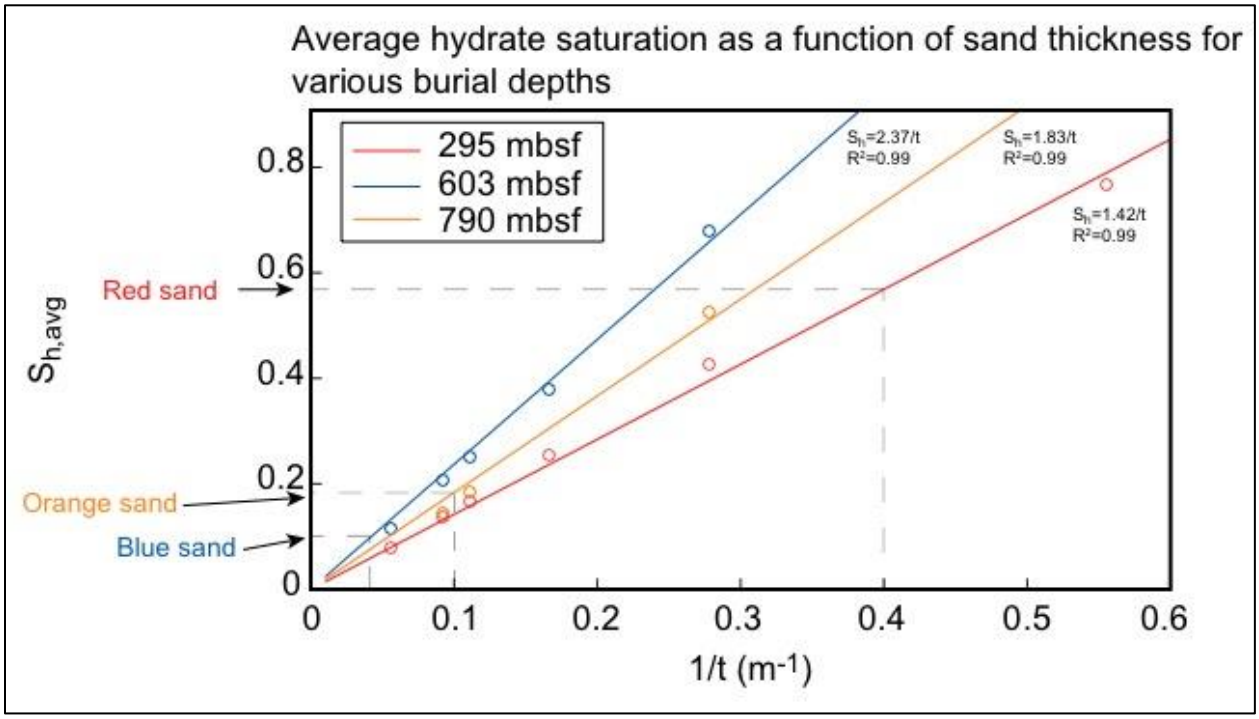

Figure 8. Average hydrate saturation as a function of sand thickness for various burial depths.

Considering the WR313H well, dashed gray lines indicate the approximate depths and thicknesses of the Red, Blue, and Orange sands. One-dimensional modeling results indicated for a 2.5 m-thick Red sand buried to 295 mbsf, the average hydrate saturation in the sand should approach about 60% (Figure 8), if all hydrate were produced as the result of a diffusive migration mechanism. This is consistent with what is observed by Cook and Malinverno (2013). On the other hand, for a 25 m-thick Blue sand and a 10.5 m-thick Orange sand, simulation results indicate that diffusion alone can produce about 10% and 20% average hydrate saturations in each interval, respectively. This is significantly less hydrate than is actually observed in these intervals (an average of about 60% in the Blue sand and 65% in the Orange sand).

The results of these models indicate that (1) diffusion is likely not the only methane migration mechanism at play in the thick, deeply buried sands of the Terrebonne Basin; (2) heterogeneities within sand layers could be enhancing diffusive methane flux to coarse-grained intervals; and/or (3) microbial methanogenesis cannot be represented as simplistically as in this study. In the Blue sand, which is characterized by significant fine-grained interbedding between hydrate accumulations in coarse-grained intervals, methane solubility gradients between thin laminations could enhance methane transport within the sand unit and thus bolster hydrate growth in the unit's coarser-grained sections. Such fine-scale heterogeneities are not currently captured but are the subject of future work. The Orange sand, however, occurs deeper and is made up of much

less interbedding than the Blue sand. It is likely that advective transport due to long-range gas transport and/or overpressuring is enhancing hydrate accumulations in this unit.

Two-dimensional Lagrangian simulations of a dipping sand layer

Two-dimensional simulations performed in this study bury a thin, dipping tabular sand body through the hydrate stability zone in a reference frame with time-varying boundary conditions. Boundary conditions are formulated in the same way as described for 1D simulations. The sand is maintained as a flat dipping surface by rotating the gravity vector with respect to the simulation domain. This is important in a discrete sense on a small scale because in a rectangular grid system oriented orthogonally to gravity, the edge of a dipping sand must be described by a discrete step function, across which diffusion can act laterally and vertically. When the scale of grid discretization is on a similar order of magnitude to the thickness of the sand itself, a jagged sand edge created by discretizing limitations could yield unwanted methane diffusion parallel to the sand surface.

Depicted in Figure 9, we use 2D simulations to explore how sand-clay concentration gradients along a portion of a dipping sand affect gas hydrate accumulations in and around the sand layer. As in 1D simulations, methane is generated microbially in clays as an exponentially decaying function of depth. If enough methane is generated in the clays to exceed the solubility of the sand, a clay-sand concentration gradient drives diffusive methane flux into the sand. During earlier stages of burial (Figure 9a), when methane input due to microbial methanogenesis outpaces the increase in methane solubility of the system with burial, gas hydrate growth proceeds in both the sand layer and the bounding clay, but a hydrate free zone separates hydrate accumulations in both sections.

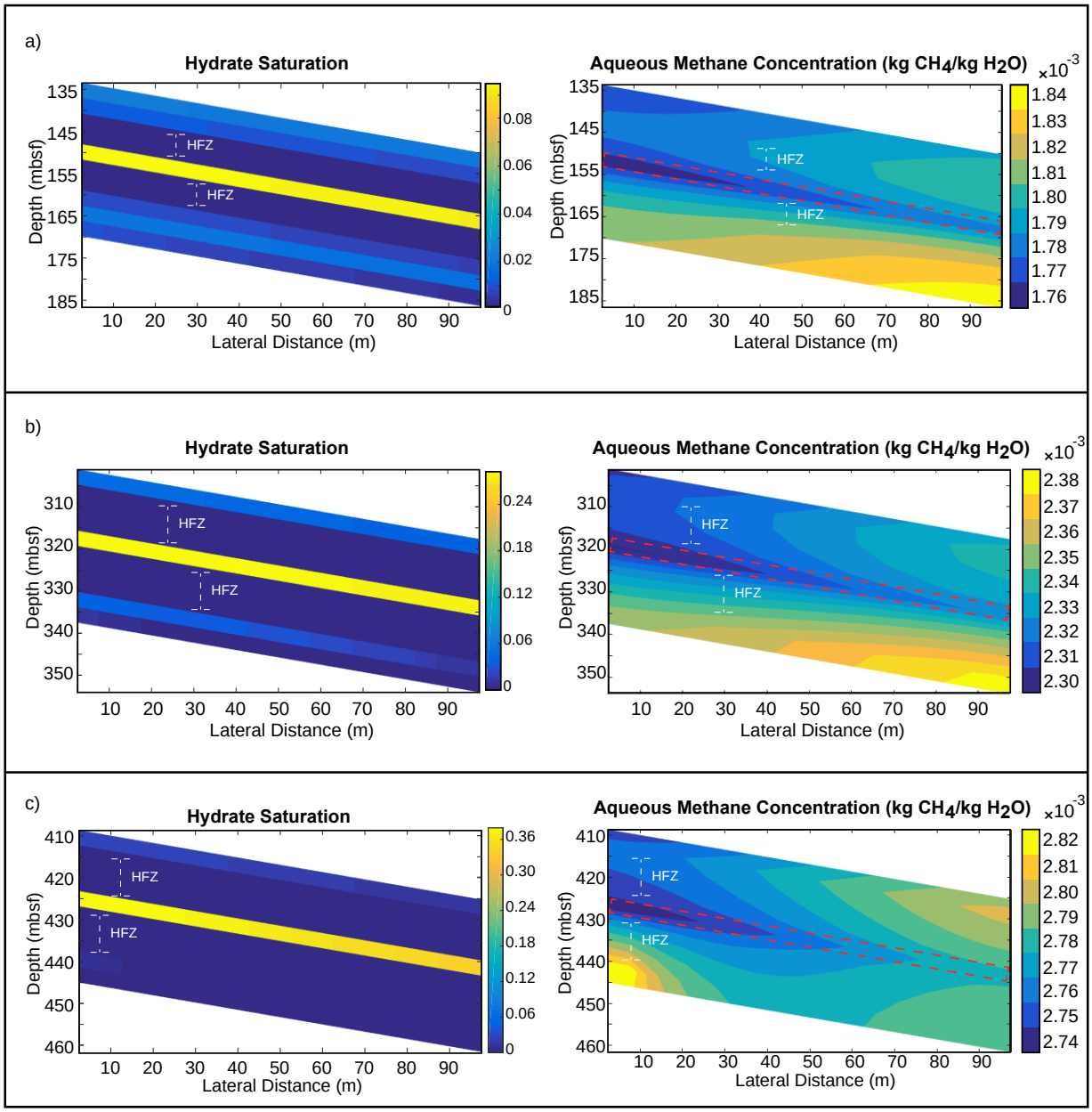

Figure 9. Simulated hydrate saturations, separated by hydrate free zones (HFZ), and dissolved methane concentrations in a dipping, 3.6 m-thick sand layer as it is buried through the hydrate stability zone at different stages of burial.

Everywhere in the system, dissolved methane concentrations increase downdip (Figure 9). However, perpendicular to the sand the direction of the concentration gradient changes. Beneath the sand, dissolved methane concentrations decrease as they approach the sand (as a result of sand-clay variations in solubility), resulting in net methane transport up toward the sand. Immediately above the sand, net methane transport is down toward the sand when hydrate exists

in the bounding clay because dissolved methane concentrations decrease toward the sand. The direction of methane transport changes again, however, at the upper end of the hydrate free zone because methane solubility in the hydrate-bearing clay decreases with decreasing depth.

As the system is buried, the sand-clay solubility difference at the downdip end of the sand increases at a faster rate than updip because the depth-wise rate of change in solubility increases with increasing depth (Xu and Ruppel, 1999). In combination with a decreasing methane input due to methanogenesis, this effect causes hydrate to dissociate in the clay downdip and beneath the sand faster than updip and above the sand. Dissociation occurs in the clay both above and below the sand layer, but the sand layer is shielded from dissociation while hydrate exists in the nearby clay because the gradient in methane concentration within the hydrate free zones always directs methane transport toward the sand (Figure 9b). As is illustrated in Figure 9c, hydrate dissociates fully first downdip and beneath the sand. A region of high methane concentration still exists updip where the clay layer contains very low hydrate saturations. Since hydrate is absent in the clay downdip beneath the sand, hydrate within the sand begins to dissociate downdip.
At all stages of the 2D simulations, hydrate saturations are significantly lower than those predicted in 1D simulations. In 2D, a 3.6 m-thick sand layer buried to 295 mbsf accumulates an average hydrate saturation of 24%. One-dimensional modeling suggests (Figure 8) that the average hydrate saturation in this sand should equal 1.42/3.6, or about 39% hydrate saturation.

The discrepancy between 1D and 2D models is likely due primarily to the fact that 2D simulations can capture the aqueous methane concentration gradient in two directions as opposed to one. In 1D models, the aqueous methane concentration gradient is required to be oriented perpendicular to the sand. In 2D, however, there can be a concentration gradient not only perpendicular to the sand but also updip within the clay and the sand layers, as is illustrated in Figure 9. This ultimately leads to less diffusive methane transport to dipping sand grid blocks in 2D as compared to 1D.

Although these 2D simulations are helpful for better understanding the multidimensional nature of aqueous methane concentration gradients in diffusion-dominated systems, the sand modeled here spans only about 10 m in depth. This model therefore does not adequately demonstrate differences in hydrate saturation along the dip of a sand body spanning greater depths; for this we instead look to 3D simulations.

Basin-scale three-dimensional simulations

We employed 3D basin-scale modeling to better understand how, on a regional scale, gas hydrate distribution in a diffusion-dominated system could be influenced by basin geometry. The top boundary is set at seafloor hydrostatic pressure, the bottom boundary condition is that of constant advective compaction flux, and constant temperature boundary conditions are defined by the geothermal gradient. By directly incorporating the results of 3D seismic interpretation, hydrate

growth is tracked in four distinct sand layers as they are buried and rotated through the hydrate stability zone in a fixed reference frame. Sand layers imported in these simulations extend about 30 km2 down through the hydrate stability zone and exhibit dip as well as curvature. Three-dimensional modeling is therefore able to demonstrate spatial variation of gas hydrate saturations in sand layers in a way that is not possible in 1D and 2D. Additionally, a further benefit of modeling in 3D is that it can capture the interaction potential between multiple dipping sands whose orientation to one another changes in space and time.

The results of 3D seismic interpretation from the Terrebonne Basin to distinguish sand layers is incorporated into 3D simulations to produce synthetic hydrate saturation profiles using realistic stratigraphic relationships between sands. Horizons interpreted from seismic data, which delineate the top and bottom surface of sand layers, are imported directly into the simulator and mapped from WGS 84, UTM 15N (EPSG: 32615) coordinate system to grid blocks in the simulation environment (Figure 10).

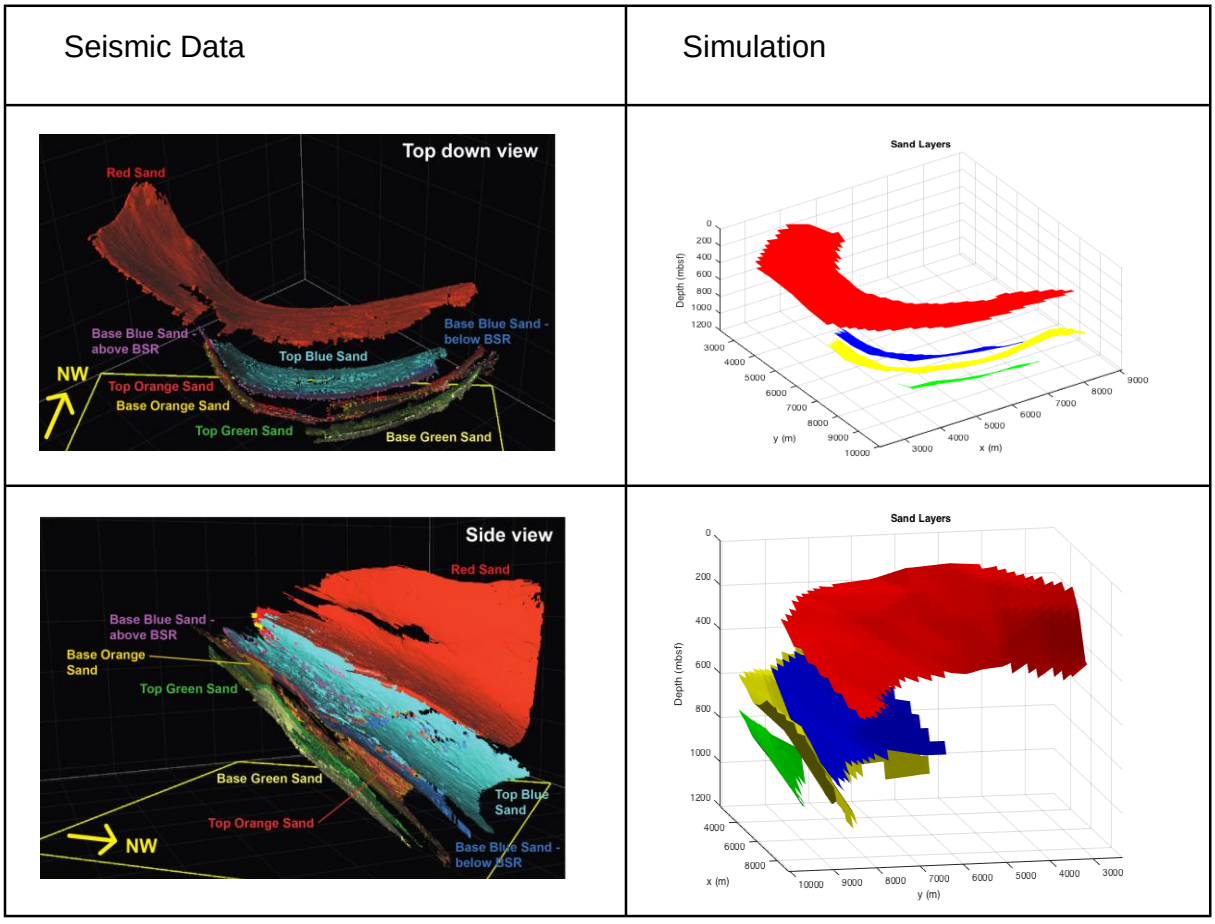

Figure 10. Three-dimensional perspective of interpreted sand horizons, which are imported into the simulator.

As depicted in Figure 11b, full-scale 3D modeling yields similar hydrate growth patterns to those seen in 1D and 2D models: hydrate saturations in deeply buried sands increase with depth, but at a certain depth of burial, hydrate begins to dissociate. In 3D simulations, hydrate also accumulates in higher saturations downdip because the sand-clay solubility contrast is larger at depth. Although the sand layers comprising methane hydrate reservoirs of interest to this study are nearly planar, they do exhibit some curvature, tend to converge toward each other, and thin out in the updip direction. There is a noticeable absence of significant hydrate accumulation in the topmost sand layer near where it is closest to the sand layer beneath it. The close proximity of the two sand layers could create competition for diffusion of methane from the clay between them; if the clay layer between the two sands were not thick enough, neither of the sand layers would be able to soak up methane to their maximum potential. This finding suggests that while planar geometries may yield close approximations of hydrate distributions on a regional scale, using 2D cross sections to model multilayered hydrate systems could overestimate hydrate saturations if sand layers converge out of plane.

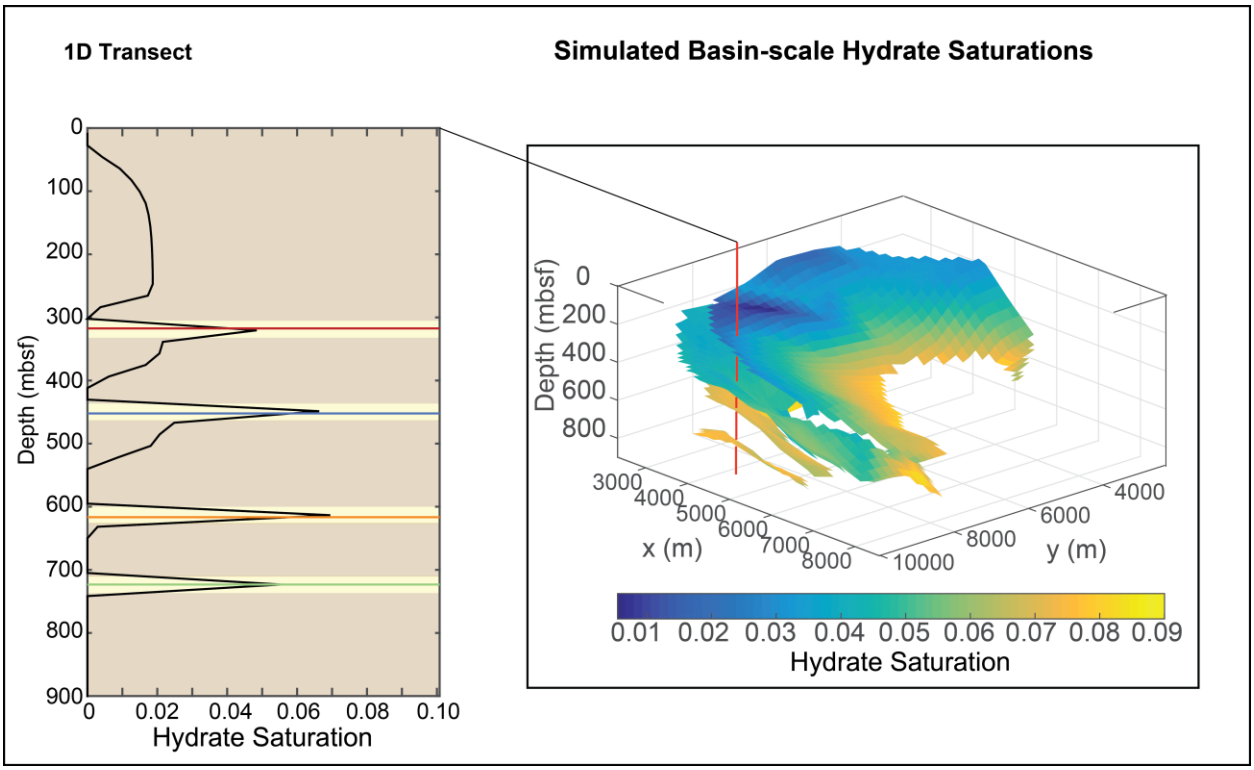

Figure 11. Three-dimensional simulated gas hydrate saturations in 4 sand layers (18.3 m-thick), accompanied by a 1D transect. In the 1D transect, sand layers are highlighted in yellow, and clays are highlighted in brown.

Comparing regional trends to a 1D transect (Figure 11a), it is easier to see how, deep in the sediment column, an increase in methane solubility with burial begins to dissociate gas hydrate present in sand layers (as was seen in prior 1D and 2D simulations). During burial, while hydrate

still exists in clays surrounding the sands, the sand layers still appear to experience net hydrate growth. When hydrate in the clay layers completely dissociates due to increasing methane solubility with burial, hydrate saturations in the sands then begins to diminish. This confirms the effect seen in 1D and 2D simulations on a regional scale and further implies that hydrate-filled clay intervals could be associated with preserved hydrate accumulations in nearby hydraulically connected sands. Preservation of high hydrate saturations at depth may require an additional advective component of methane supply in the absence of hydrate-bearing clay nearby.

Table 1.

Variable name	**1D and 2D Lagrangian**	**3D Eulerian**
Seafloor Depth [m]	1917	1917
Seafloor Temperature [^{o}C]	4.85	4.85
Geothermal Gradient [^{o}C/km]	19	19
BHSZ [m]	900	900
D_s [m^2/s]	1x10^{-10}	1x10^{-10}
Dip angle (2D only) [degrees]	10	n/a
Gravitational acceleration [m/s^2]	9.8	9.8
T_f [K]	273.15	273.15
v_f [mm/yr]	variable	1
k_α [kg/m^3]	2241	2241
λ [s^{-1}]	1x10^{-13}	1x10^{-12}
α_{SMT} [dry wt%]	0.5%	0.5%
ω [mm/yr]	1.0	1.0
z_{SMT} [m]	10	10
T_{mb} [K]	273.15	273.15
σ_{hl} [N/m]	0.027	0.027
θ [degrees]	0^o	0^o

H_f [kJ/kg]	439	439
ρ_h [kg/m^3]	925	925
r_{sand} [microns]	n/a	1
r_{cmax} [microns]	0.2	n/a
r_{clay} [microns]	n/a	0.01
σ_r [microns]	20	n/a
r_m [microns]	20	n/a

Li Wei and Ann Cook have been working on her 1D model, and trying different approaches to model the 2.5 m sand interval within the fracture layer at Walker Ridge. She submitted an abstract along with Cook, Daigle, Malinverno, Nole and others to the 2017 ICGH conference on her model. Li presented her work at the GIMS conference in Norway and won best student poster for her session!

In the third quarter of 2016, A. Malinverno applied a time-dependent reaction-transport model to compute predicted gas hydrate contents in fine-grained sediments. In these sediments, hydrates in veins and fractures have been observed within discrete depth intervals that are not connected to deep methane sources and therefore are likely sourced from in situ microbial methane. Methane sources and hydrate formation in these fine-grained sediments is important to understand the accumulation of hydrates in adjacent coarse-grained layers. The modeling shows that transient high organic carbon deposition at the seafloor can result in more intense methane generation during burial and enhanced hydrate formation in isolated depth intervals.

Specific objectives

Milestones 2.A, 2.B, and 2.C were scheduled to be completed this quarter. The milestones were met; details are given in the quarterly report dated July 28th 2016.

Significant results and key outcomes

We have shown that diffusion of microbial methane into sand layers can result in high hydrate saturations, but that the organic inputs necessary to achieve these hydrate saturations may not be sustainable over geologic time.

We have shown that updip advection may be able to produce the observed hydrate saturations, but results in a heterogeneous accumulation of hydrate with the highest hydrate saturations at the downdip limits of sands.

We have shown that a combination of advection and microbial methanogenesis can result in a more uniform hydrate distribution in sands, with high hydrate saturation.

We have shown that at depth, high hydrate saturations in sands can be preserved if bounding clays contain hydrate or at least contain methane in concentrations above the solubility of the sand layer. If these conditions are not met, it is likely that high hydrate saturations in sand intervals are the result of advection being the dominant methane transport mechanism.

Two-dimensional simulations demonstrate that in a dipping sand layer in a diffusion-dominant environment, hydrate tends to accumulate along the sand's dip and is separated from hydrate-filled clays by hydrate free zones above and below. Over time, methane solubility downdip increases faster than updip, so hydrate in the clay intervals tends to dissociate faster downdip and below the sand. Concentration gradients exist parallel and perpendicular to the sand, so less methane is transported to the sands overall in 2D and 3D simulations as compared to 1D. In 3D, simulations clearly illustrate that on a regional scale, hydrate saturations tend to focus downdip because of a stronger sand-clay solubility contrast at depth. While 3D simulations confirm the observation in 1D that hydrate in clays can preserve high hydrate saturations in sand through burial, they also demonstrate that convergence of sand layers in multilayered systems can lead to anomalous reductions in hydrate saturation due to competitive diffusion.

Other potentially important drivers of hydrate growth in thin sand layers buried within a diffusion-dominant gas hydrate system include gradients in lithology between clays and sands, time-varying rates of microbial methanogenesis, and changes in the pore water methane diffusion coefficient with variable hydrate saturation. Our simulations indicate that sand with small median pore sizes and broad pore size distributions can push hydrate growth toward the center of a sand layer. In future work we will incorporate a gradient in lithology between clay and sand instead of describing our system as containing either sand or clay lithology; we should similarly see enhanced methane transport from the edges of sands toward their center. Furthermore, incorporating a time-dependent rate of microbial methanogenesis may more accurately represent different depositional environments with different concentrations of organic carbon and methanogens of varying metabolism. Finally, because increased pore-filling hydrate saturations make pore space more tortuous, the diffusion coefficient of methane in water decreases with increasing hydrate saturation. Incorporating this effect into simulations would slow the process of diffusion with increasing hydrate saturation, thus potentially diminishing the total amount of gas hydrate that can accumulate at the edges of a sand layer.

What opportunities for training and professional development has the project provided?

PI Daigle and co-PI Mohanty have been working with PhD student Michael Nole on various aspects of pore-scale modeling of methane hydrate systems. This work has involved weekly meetings and independent work.

Co-PIs Cook and Malinverno have been working with PhD student Li Wei on modeling microbial methanogenesis. This work has involved weekly meetings and independent work.

How have the results been disseminated to communities of interest?

Three presentations were made at the Gas in Marine Sediments Conference in Tromsø, Norway. One manuscript was published in *Geophysical Research Letters*.

Plans during next reporting period to accomplish goals

Work will commence on Tasks 5.1, 5.2, and 5.3.

PRODUCTS

Hillman, J.I.T., Cook, A.E., Daigle, H., Nole, M., Malinverno, A., 2016. Determining gas hydrate distribution in sands using integrated analysis of well log and seismic data in the Terrebonne Basin, Gulf of Mexico. Presented at the Gas in Marine Sediments Conference, Tromsø, Norway, 19-22 September 2016. Federal support acknowledged.

Malinverno, A., Cook, A., Daigle, H., 2016. Modeling the formation of methane hydrate-bearing intervals in fine-grained sediments. Presented at the Gas in Marine Sediments Conference, Tromsø, Norway, 19-22 September 2016. Federal support acknowledged.

Nole, M., Daigle, H., Cook, A., Malinverno, A., 2016. Short-range, overpressure-driven methane migration in coarse-grained gas hydrate reservoirs. *Geophysical Research Letters*, vol. 43, no. 18, pp. 9500-9508. Federal support acknowledged.

Nole, M., Daigle, H., Cook, A., Malinverno, A., 2016. The impact of flow focusing on gas hydrate accumulations in overpressured marine sediments. Presented at the Gas in Marine Sediments Conference, Tromsø, Norway, 19-22 September 2016. Federal support acknowledged.

PARTICIPANTS AND OTHER COLLABORATING ORGANIZATIONS

Name: Hugh Daigle

Project role: PI
Nearest person month worked: 1
Contribution to project: Project management; assisted with code development
Collaborated with individual in foreign country: No

Name: Kishore Mohanty
Project role: Co-PI
Nearest person month worked: 1
Contribution to project: Assisted with code development
Collaborated with individual in foreign country: No

Name: Steven Bryant
Project role: Co-PI
Nearest person month worked: 1
Contribution to project: Assisted with code development
Collaborated with individual in foreign country: No

Name: Michael Nole
Project role: Graduate Student
Nearest person month worked: 3
Contribution to project: Primary worker on developing computer code
Collaborated with individual in foreign country: No

Name: Ann Cook
Project role: Co-PI
Nearest person month worked: 1
Contribution to project: Worked on gathering specific data for modeling of microbial methanogenesis, developing methanogenesis code
Collaborated with individual in foreign country: No

Name: Li Wei
Project role: Graduate Student
Nearest person month worked: 3
Contribution to project: Worked on developing methanogenesis code
Collaborated with individual in foreign country: No

Name: Alberto Malinverno
Project role: Co-PI
Nearest person month worked: 1
Contribution to project: Provided data for microbial methanogenesis modeling

Collaborated with individual in foreign country: No

IMPACT

What is the impact on the development of the principal discipline of the project?

The central focus of this project is refining our understanding of the methane migration pathways that feed methane hydrate deposits in marine sediments. Understanding migration pathways is an important component of understanding methane hydrates as a petroleum system, a necessary step towards prospecting for economically recoverable hydrate deposits. Additionally, our results will help refine our understanding of the carbon cycle in marine sediments, and specifically how methane is transported and sequestered.

What is the impact on other disciplines?

The results of this project will be important for other engineering disciplines in which researchers are developing methods for extracting methane from the subsurface since it will provide information on how methane is distributed in sediments at different scales. In addition, the results will be of interest to the economics and risk assessment fields since we will develop methods to determine more precisely how much hydrate may be present in subsurface reservoirs.

What is the impact on the development of human resources?

This project will provide funding for three graduate students to conduct collaborative research on methane hydrates and give them an opportunity to participate in important hands-on learning experiences outside the classroom.

What is the impact on physical, institutional, and information resources that form infrastructure?

Our results may be used for better design of subsea oil and gas infrastructure since more precise assessment of hydrate resources will allow better assessment of hydrates as a hazard. In addition, production infrastructure specifically for hydrate reservoirs may be improved by our results since we will allow more accurate determination of the volumes of methane expected to exist in the subsurface.

What is the impact on technology transfer?

Our results will be disseminated at conferences and in peer-reviewed publications.

What is the impact on society beyond science and technology?

The impact of this work on society will be twofold. First, the better understanding of hydrates in a petroleum systems framework will allow for more efficient production of natural gas from these deposits, which will provide an additional energy resource. Second, the better understanding of methane cycling and distribution in the subsurface will influence regulatory decisions involving hydrates as geohazards or climate change agents.

What dollar amount of the award's budget is being spent in foreign country(ies)?
None

CHANGES/PROBLEMS
None

SPECIAL REPORTING REQUIREMENTS
None

BUDGETARY INFORMATION
See attached spreadsheet.

References

Bhatnagar, G., Chapman, W.G., Dickens, G.R., Dugan, B., Hirasaki, G.J., 2007. Generalization of gas hydrate distribution and saturation in marine sediments by scaling of thermodynamic and transport processes. Am. J. Sci., 307, 861-900.

Bihani, A., Daigle, H., Cook, A., Glosser, D., Shushtarian, A., 2015. Pore size distribution and methane equilibrium conditions at Walker Ridge Block 313, northern Gulf of Mexico, abstract OS23B-1999, American Geophysical Union Fall Meeting, San Francisco, CA, 15 December 2015.

Clennell, M.B., Hovland, M., Booth, J.S., Henry, P., Winters, W.J., 1999. Formation of natural gas hydrates in marine sediments 1. Conceptual model of gas hydrate growth conditioned by host sediment properties. J. Geophys. Res., 104(B10), 22985-23003.

Cook, A.E., Malinverno, A., 2013. Short migration of methane into a gas hydrate-bearing sand layer at Walker Ridge, Gulf of Mexico. Geochem. Geophys. Geosyst., 14(2), 283-291.

Daigle, H., 2011. Pore-scale controls on permeability, fluid flow, and methane hydrate distribution in fine-grained sediments. PhD thesis, Rice University, Houston, Texas, USA.

Daigle, H., Dugan, B., 2010. Origin and evolution of fracture-hosted methane hydrate deposits. J. Geophys. Res., 115, B11103.

Daigle, H., Dugan, B., 2014. Data report: permeability, consolidation, stress state, and pore system characteristics of sediments from Sites C0011, C0012, and C0018 of the Nankai Trough. In: Henry, P., Kanamatsu, T., Moe, K.T., the Expedition 333 Scientists (Eds.), Proceedings of the

Integrated Ocean Drilling Program 333. Integrated Ocean Drilling Program Management International, Tokyo, 1-23.
Day-Stirrat, R.J., Flemings, P.B., You, Y., Aplin, A.C., van der Pluijm, B.A., 2012. The fabric of consolidation in Gulf of Mexico mudstones. Marine Geology 295-298, 77-85.
Frye, M., 2008. Preliminary evaluation of in-place gas hydrate resources: Gulf of Mexico Outer Continental Shelf. Minerals Management Service Report 2008-004. Available online at: http://www.boem.gov/uploadedFiles/BOEM/Oil_and_Gas_Energy_Program/Resource_Evaluation/Gas_Hydrates/MMS2008-004.pdf
Gordon, D.S., Flemings, P.B., 1998. Generation of overpressure and compaction-driven fluid flow in a Plio-Pleistocene growth-faulted basin, Eugene Island 330, offshore Louisiana. Basin Res., 10(2), 177-196.
Handa, Y.P., 1990. Effect of hydrostatic pressure and salinity on the stability of gas hydrates. J. Phys. Chem., 94(6), 2652-2657.
Henry, P., Thomas, M., Clennell, M.B., 1999. Formation of natural gas hydrates in marine sediments 2. Thermodynamic calculations of stability conditions in porous sediments. Journal of Geophysical Research 104(B10), 23005-23022.
Hutchinson, D.R., Hart, P.E., Collett, T.S., Edwards, K.M., Twichell, D.C., Snyder, F., 2008. Geologic framework of the 2005 Keathley Canyon gas hydrate research well, northern Gulf of Mexico. Marine and Petroleum Geology 25(9), 906-918.
Liu, X., Flemings, P.B., 2011. Capillary effects on hydrate stability in marine sediments. Journal of Geophysical Research 116, B07102.
Malinverno, A., 2010. Marine gas hydrates in thin sand layers that soak up microbial methane. Earth Planet. Sci. Lett., 292(3-4), 399-408.
Malinverno, A., Goldberg, D, 2015. Testing short-range migration of microbial methane as a hydrate formation mechanism: Results from Andaman Sea and Kumano Basin drill sites and global implications. Earth Planet. Sci. Lett., 422, 105-114.
Nole, M., Daigle, H., Milliken, K.L., Prodanović, M., 2016. A method for estimating microporosity of fine-grained sediments and sedimentary rocks via scanning electron microscope image analysis. Sedimentology, in press.
Sun, X., Mohanty, K.K., 2006. Kinetic simulation of methane hydrate formation and dissociation in porous media. Chem. Eng. Sci., 61(11), 3476-3495.

Baseline Reporting Quarter	Budget Period 1																	
	Q1		Q2		Q3		Q4		Q1		Q2		Q3		Q4			
	10/1/13 - 12/31/13		1/1/14 - 3/31/14		4/1/14 - 6/30/14		7/1/14 - 9/30/14		10/1/14 - 12/31/14		1/1/15 - 3/31/15		4/1/15 - 6/30/15		7/1/15 -			
	Q1	Cumulative Total	Q2	Cumulative Total	Q3	Cumulative Total	Q4	Cumulative Total	Q1	Cumulative Total	Q2	Cumulative Total	Q3	Cumulative Total	Q4			
Baseline Cost Plan																		
Federal Share	$ 97,167	$ 97,167	$ 97,167	$ 194,333	$ 97,167	$ 291,500	$ 97,167	$ 388,666	$ 97,167	$ 485,833	$ 97,167	$ 582,999	$ 108,258	$ 691,257	$ 108,258			
Non-Federal Share	$ 24,292	$ 24,292	$ 24,292	$ 48,583	$ 24,292	$ 72,875	$ 24,292	$ 97,167	$ 24,292	$ 121,458	$ 24,292	$ 145,750	$ 29,698	$ 175,447	$ 29,698			
Total Planned	$ 121,458	$ 121,458	$ 121,458	$ 242,916	$ 121,458	$ 364,374	$ 121,458	$ 485,833	$ 121,458	$ 607,291	$ 121,458	$ 728,749	$ 137,956	$ 866,704	$ 137,956			
Actual Incurred Cost																		
Federal Share	0	0	$ 4,053	$ 4,053	$ 59,844	$ 63,897	$ 135,066	$ 198,963	$ 113,678	$ 312,641	$ 174,686	$ 487,327	$ 36,292	$ 523,619	$ 179,321			
Non-Federal Share	0	0	0	0	$ -	$ -	$ 8,832	$ 8,832	$ 63,148	$ 71,980	$ 51,748	$ 123,728	$ 6,615	$ 130,343	$ 21,898			
Total Incurred Costs	0	0	0	0	$ 59,844	$ 63,897	$ 143,898	$ 207,795	$ 176,826	$ 384,621	$ 226,435	$ 611,056	$ 42,907	$ 653,963	$ 201,219			
Variance																		
Federal Share	$ (97,167)	$ (97,167)	$ (93,113)	$ (190,280)	$ (37,323)	$ (227,602)	$ 37,900	$ (189,703)	$ 16,512	$ (173,191)	$ 77,520	$ (95,672)	$ (71,966)	$ (167,638)	$ 71,063			
Non-Federal Share	$ (24,292)	$ (24,292)	$ (24,292)	$ (48,583)	$ (24,292)	$ (72,875)	$ (15,460)	$ (88,335)	$ 38,856	$ (49,478)	$ 27,457	$ (22,021)	$ (23,083)	$ (45,104)	$ (7,800)			
Total Variance	$ (121,458)	$ (121,458)	$ (117,405)	$ (238,863)	$ (61,614)	$ (300,477)	$ 22,440	$ (278,037)	$ 55,368	$ (222,670)	$ 104,977	$ (117,693)	$ (95,049)	$ (212,742)	$ 63,263			

Budget Period 2										Budget Period 3							
4	Q1		Q2		Q3		Q4		Q1		Q2		Q3		Q4	
9/30/15	10/1/15 - 12/31/15		1/1/16 - 3/31/16		4/1/16 - 6/30/16		7/1/16 - 9/30/16		10/1/16 - 12/31/16		1/1/17 - 3/31/17		4/1/17 - 6/30/17		7/1/17 - 9/30/17	
Cumulative Total	Q1	Cumulative Total	Q2	Cumulative Total	Q3	Cumulative Total	Q4	Cumulative Total	Q1	Cumulative Total	Q2	Cumulative Total	Q3	Cumulative Total	Q4	Cumulative Total
$ 799,515	$ 108,258	$ 907,773	$ 108,258	$ 1,016,031	$ 108,258	$ 1,124,289	$ 108,258	$ 1,232,547	$ 111,371	$ 1,343,918	$ 111,371	$ 1,455,290	$ 111,371	$ 1,566,661	$ 111,371	$ 1,678,032
$ 205,145	$ 29,698	$ 234,842	$ 29,698	$ 264,540	$ 29,698	$ 294,237	$ 29,698	$ 323,935	$ 30,888	$ 354,823	$ 30,888	$ 385,711	$ 30,888	$ 416,600	$ 30,888	$ 447,488
$ 1,004,660	$ 137,956	$ 1,142,615	$ 137,956	$ 1,280,571	$ 137,956	$ 1,418,526	$ 137,956	$ 1,556,482	$ 142,260	$ 1,698,741	$ 142,260	$ 1,841,001	$ 142,260	$ 1,983,260	$ 142,260	$ 2,125,520
$ 702,941	$ 142,071	$ 845,012	$ 112,450	$ 957,462	$ 85,549	$ 1,043,011	$ 133,581	$ 1,176,592								
$ 152,241	$ 21,898	$ 174,139	$ 14,224	$ 188,363	$ 72,390	$ 260,753	$ 38,937	$ 299,689								
$ 855,182	$ 163,969	$ 1,019,151	$ 126,674	$ 1,145,825	$ 157,939	$ 1,303,764	$ 172,518	$ 1,476,282								
$ (96,574)	$ 33,813	$ (62,761)	$ 4,192	$ (58,569)	$ (22,709)	$ (81,278)	$ 25,323	$ (55,955)								
$ (52,904)	$ (7,800)	$ (60,704)	$ (15,474)	$ (76,177)	$ 42,693	$ (33,485)	$ 9,239	$ (24,246)								
$ (149,478)	$ 26,014	$ (123,464)	$ (11,281)	$ (134,746)	$ 19,984	$ (114,762)	$ 34,562	$ (80,200)								